ELSEVIER

Nuclear Engineering and Design 146 (1994) 35–42

Nuclear Engineering and Design

# Impedance based flow reconstruction – A novel flow composition measuring technique for multi-phase-flows

F. Klug, F. Mayinger

*Lehrstuhl A f. Thermodynamik, Techn. Univ. München, RFG, Postfach 10 20 24, 80333 München 2, Germany*

**Abstract**

In this paper, experimental data obtained with a new impedance based measuring technique for multi-phase flows are presented. By impedance measurement between different electrode combinations of a completely non-intrusive, multi-electrode impedance probe, a vector is obtained, which is subsequently compared to a set of stored data, shaped as a reference matrix. This allows for the on-line reconstruction of the local volumetric flow composition and the occurring flow regime. The method covers component concentrations in the range of 0–100% over multiple flow regimes and a wide field of flow components. In addition to a brief description of the reconstruction principle, different ways of generating the reference matrix are discussed and measured data for oil, water and gas flows are presented. Component concentration can be determined at an overall accuracy better than 2%.

## 1. Impedance method

The impedance method is widely applied for measurement of volumetric concentrations in multiphase flows. It is based on the different electrical properties (permittivity, conductivity) of the flow components and their effect on the measured impedance (capacitance, conductance) of an appropriate sensor. The majority of these applications comes from the field of two-phase flows, and especially from capacitance measurement in non-conducting fluids. Although the impedance method offers a number of advantages like simultaneous answer and no need for moving parts, its sensitivity to the flow pattern sometimes limits the range of application. Many different electrode designs have been developed, trying to minimize this limitation. A popular method is the use of parallel plate electrodes, Auracher [1]. The use of ring electrodes is described by Andreussi et al. [2], helical electrodes have been tested by Geraets et al. [3], Abouelwafa et al. [4]. A method of electrode excitation was proposed by Merilo et al. [5] and incorporates the use of 6 strip-electrodes fed by a 3-phase voltage generator.

For the generally occurring flow conditions, especially with dispersed flow components, a number of analytical formulae are known, which connect the permittivity $\varepsilon$ of a mixture of two fluids of particular permittivities $\varepsilon_1$, $\varepsilon_2$ with their volumetric concentration ratio. These models are based on general conditions regarding the shape of the dispersed particles and often are limited to relatively small maximum concentrations. The most popular models are those by e.g. Maxwell


*SSDI* 0029-5493(93)E0218-9

[6], Bruggemann [7], a very good review is given by van Beek [8]. Dykesteen et al. [9] have proposed a method of determining the component concentrations in 3-component flows by measuring both the capacitance and the resistance of an impedance sensor.

The sensitivity of the impedance to the distribution pattern of the components within the sensor leads to different calibration curves for each flow regime. In many practical flow situations, these curves differ very much. In order to avoid large errors, this calls for more information about the dominating flow pattern.

## 2. Reconstruction principle

To overcome the insufficiencies mentioned above, a new approach is made for concentration measurement in multi-phase flows [10]. Although the proposed method has been originally developed with respect to offshore applications in oil/water/gas-mixtures, it can be easily applied to a much wider field of multi-component flows. The main part of the described measuring technique is a non-intrusive impedance probe consisting of eight surface-plate electrodes mounted on the inner side of the tube (see Fig. 1).

With this probe, the impedance between different combinations of electrodes – the so-called measuring fields – is measured. For every measuring field, the impedance – as an integral parameter – is determined by the component distribution within the *whole* sensing volume of the probe. However, the individual domains of the sensing volume make different contributions to the total amount of the flow-influenced probe impedance. Therefore, characteristic distribution patterns for the spacial sensitivity [11] can be observed, which allows one to classify the multitude of measuring fields into several groups.

Each group consists of a certain number of fields, which depends upon the degree of field symmetry, the fields being "rotated" against each other by an angle $\Delta\psi = k \cdot 360°/8$. These are the diametral fields $D_1$–$D_4$, eccentric $E_1$–$E_8$, wall $W_1$–$W_8$ and large fields $B_1$–$B_4$, integral fields $I_1$, $I_2$, and the Maltese-cross shaped field $M_1$, see Fig. 2. Although a much higher number of fields is theoretically possible, the conducted tests proved, that the 27 fields shown above are sufficient to ensure a good and unambiguous performance over the flow regimes of practical relevance.

Within each measurement cycle, the probe impedance for $m$ fields is recorded. This mea-

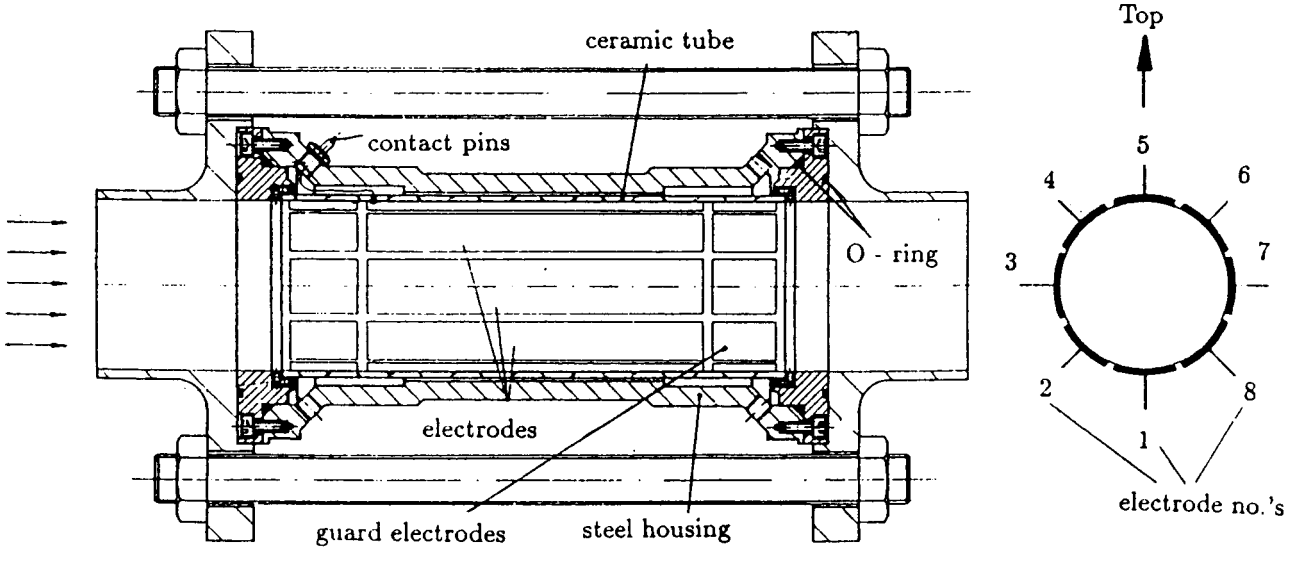


Fig. 1. Non-intrusive impedance probe (Ø54 mm, $L$ = 160 mm) with 8 surface-plate electrodes.

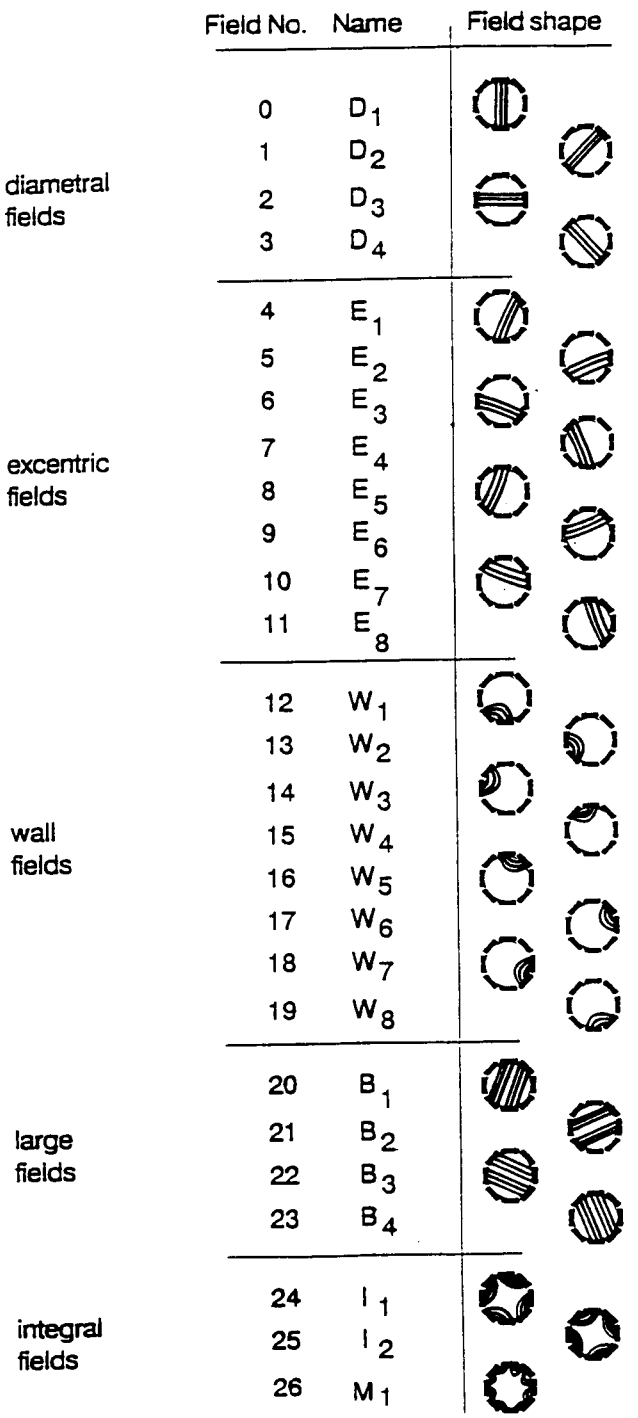


Fig. 2. Measuring fields used with the impedance probe.

surement vector $V$, consisting of $m$ impedance readings, is compared to a stored reference matrix $M$ of dimension $m \times n$. $M$ consists of the $(m \cdot n)$ impedance values representing $n$ different flow compositions over several flow regimes. Within every flow regime, the component concentration is increased gradually, the stepwidth depending on the overall accuracy of the measurement setup (typ. 2%). In this way, the column numbers contain the encoded information about the flow composition and the flow regime.

It proved useful to generate both $V$ and $M$ with normalized, relative impedance values, $0 \leqslant Z_{ij} \leqslant 1$. In the case of non- conducting fluids, with capacitance measurement, this leads to dimensionless capacitances according to

$$C^* = \frac{C_{\text{meas}} - C_{\min}}{C_{\max} - C_{\min}}. \tag{1}$$

This ensures a good comparability and achieves independence of the actual probe dimensions. In the next step, $V$ and $M$ are compared, calculating the error

$$s(j) = \sum_{i=1}^{m} \left( |V_i - M_{ij}| \right)^{1/2} \tag{2}$$

for every column of $M$. Due to the use of dimensionless impedances which lead to small error values in the range $s(j) < 1$ over most interesting flow regimes, eq. (2) shows a sharper detection of the minimum, compared to the sum over error squares, often used for this purpose. The reconstruction is finally performed by determining the best-fit column ($s(j_0) = \min\{s(j)\}$). The flow composition and the occurring flow regime are then determined by decoding the address of the such determined best-fit column $j_0$.

## 3. Generation of the reference matrix

The reference matrix can be generated in two ways: by numerical calculation or by calibration.

### 3.1. Numerical calculation

The numerical method [10], [12] is based on the solution of Poisson's equation for a domain of

permittivity $\varepsilon$ and space- charge density $\varrho$:

$$\nabla^2\varphi = \Delta\varphi = -\frac{\varrho}{\varepsilon}. \quad (3)$$

In the special case, with no free charges $\varrho$, eqn. (3) reduces to Laplace's equation

$$\Delta\varphi = 0. \quad (4)$$

$\Delta$ represents the Laplace operator and $\varphi$ describes the potential. In Cartesian coordinates, and if one of the three dimensions can be regarded infinite, eq. (4) simplifies to the expression

$$\frac{\partial^2\varphi}{\partial x^2} + \frac{\partial^2\varphi}{\partial y^2} = 0. \quad (5)$$

The calculation of the two- dimensional field can be accomplished by use of the finite-difference-method [13]. The capacitance $C_{AB}$ between any two of a given set of electrodes is determined by the existing electrical field between the assembly, i.e., by the potential distribution between the electrodes. In this way, the impedances between any electrodes can be calculated for every specified flow distribution within the probe, so that the distribution of the impedances for every measuring field is obtained.

### 3.2. Calibration

The generation of the reference matrix by calibration can be done by two ways:
- calibration under real flow conditions, and
- bullet calibration with stationary calibration apparatus.

In the first case, the impedance probe is exposed to a multiphase flow of the required flow regime and flow components. During stepwise alteration of the flow composition, the impedance values for all measuring fields are measured and stored. For this calibration procedure, a multiphase reference measurement technique – e.g. $\gamma$-ray measurement or quick-acting valves – is required as a reference for determination of the actual volumetric flow composition. In flow regimes with fluctuating component concentrations, e.g. slug flow, it has to be ensured, that representative mean values of the void fraction are recorded. If the reference matrix is generated by calibration in real flows, the flow itself can be regarded as a "black box", and no further asumptions concerning the phase distribution (e.g. entrained droplets) are required. By consequence, even "exotic" flows, e.g. high-viscous, non-newtonian flows can be covered. The maximum possible reconstruction accuracy is determined by the accuracy of the multiphase reference measurement technique used for calibration.

If multiphase test facilities are not available, a modified calibration procedure, the calibration with a stationary apparatus can be used instead. In this case, the component distribution within the probe is simulated by phantoms. This method is suited well for flow regimes with geometrically defined interface areas, especially for stratified flow or annular flow with a negligible amount of entrained liquid in the core. The calibration apparatus used for the presented measurements is shown in Fig. 3.

The impedance probe is flanged between two plexiglass planes and connected to an impedance meter. For simulation of stratified flow, the apparatus is fixed horizontally. By injecting equal amounts of liquid with the help of a syringe, the void fraction inside the apparatus is decreased in equal steps.

For simulation of annular flow, cylindrical phantoms are located inside the probe. The circular gap between phantom and probe wall is filled with a liquid of the desired permittivity. By the use of phantoms of different diameter, a number of void fractions is represented. Simulation of core flow can be achieved with the same setup, however the liquid has to be filled *inside* the phantoms. This setup also allows for the investigation of the influence of eccentric phase distributions.

It is essential, that the void fraction steps $\Delta\alpha$ between adjacent impedance vectors stored in the reference matrix remain under a certain magnitude, which is determined by the overall-accuracy of the impedance measurement (typ.: $\Delta\alpha = 2\%$). This is achieved by interpolation algorithms applied to the data obtained either by calibration or by computation.

## 4. Experimental data

The experimental data shown below have been obtained with an impedance probe –Ø54 mm, $l = 160$ mm – in the stratified, bubbly and annular flow regime. The measurements were carried out in oil/gas and water/gas flows of ambient pressure with tap water, SHELL/ONDINA 15 oil and air. The multiphase test loop (see Fig. 4) was equipped with horizontal and vertical test

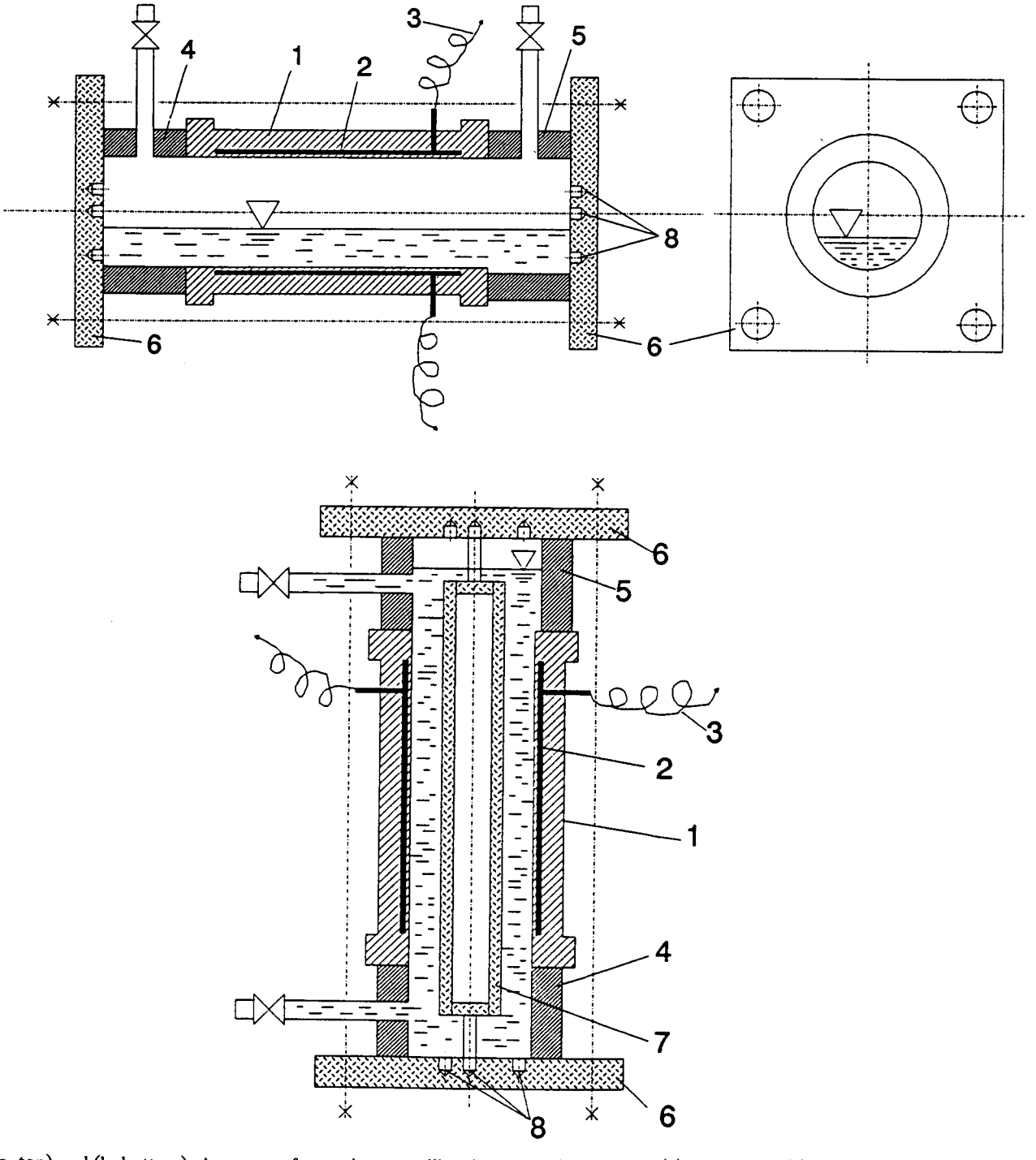


Fig. 3. (a, top) and (b, bottom): Apparatus for stationary calibration. Impedance probe (1); electrodes (2); electrical connections (3); tubes (4,5); plexiglass planes (6); phantom (7); positioning bores (8).

sections of 10 m length. Liquid flow rates could be adjusted in the range of $0.3 \leqslant \dot{V}_l \leqslant 4$ $l/s$, gas flow rates were between $0 \leqslant \dot{V}_g \leqslant 9$ $l/s$. Thus, a void fraction range of $0 \leqslant \alpha \leqslant 0.88$ could be covered. The reconstruction was based on capacitance measurement at a frequency of $f = 100$ kHz, using a HP 4284A impedance meter. This allowed for a measurement time $t_{meas} \approx 30$ ms per field, at a basic accuracy in the range of 0.1%.

According to the description of the reconstruction technique given above, it is to be expected, that the best results are obtained, if cycles with a large number of measuring fields are employed. However, this is connected with a long measuring time (up to 1.8 s) per cycle. Under many practical conditions, this is not tolerable, especially if the time history of the void fraction fluctuations has to be tracked.

In order to increase the measurement rate per cycle, a large amount of the development work on the presented new technique has therefore been spent on the composition of short cycles, composed of few fields, but nevertheless yielding a good reconstruction accuracy [10]. Generally consisting of 6–8 fields, such cycles have best performance within one certain flow regime and allow for an accuracy of up to 2–3% for void fraction determination. With the setup used, the corresponding measurement rates for these short cycles are about $2s^{-1}$ and could be considerably speeded up by the use of a faster impedance meter.

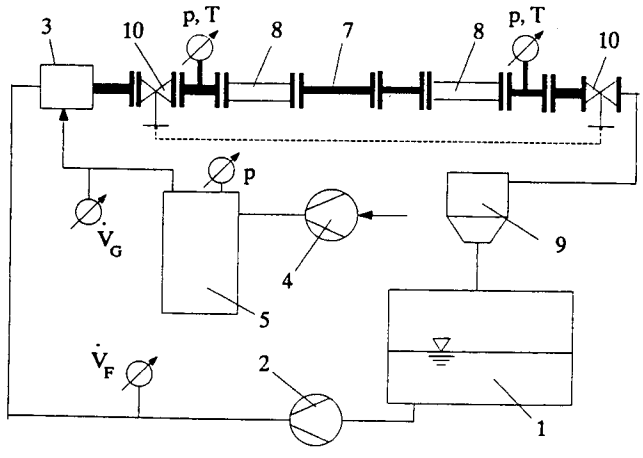


Fig. 4. Multiphase test loop. Reservoir (1); pump (2); mixer (3); compressor (4); gas tank (5); impedance probe (7); transparent sections (8); separator (9); ball valves (10).

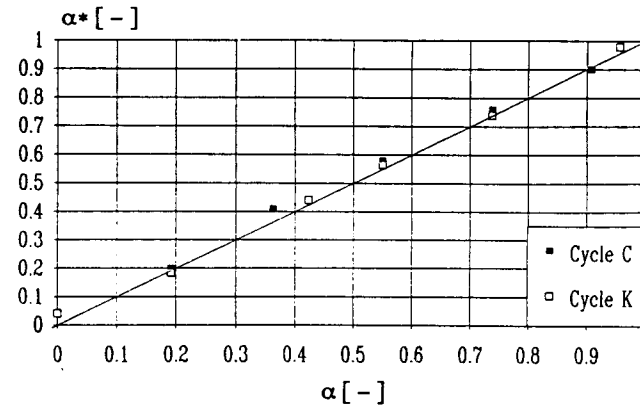


Fig. 5. Calculated ($\alpha^*$) vs. reference void fraction ($\alpha$) for stratified flow of oil/ gas. (Cycle C: 8 fields: $D_1, D_3, E_1, E_2, W_1, W_4, B_1, I_1$; Cycle K: 27 fields.)

### 4.1. Stratified flow

The good performance of the reconstruction technique for the stratified flow regime is demonstrated in Fig. 5. It shows the reconstructed void fraction $\alpha^*$ vs. the reference void fraction $\alpha$ in horizontal flow of oil and gas. $\alpha$ was determined from the liquid level measured with a transparent measuring section, containing a thin scale with etched markings. This compensates for the optical refraction in the glass wall, the reference accuracy was about 2%.

The reference matrix has been generated with the help of the stationary calibration apparatus (Fig. 3), the void fraction being changed in steps of 8%. After calibration, the "coarse" reference matrix was refined by spline interpolation to $\Delta\alpha = 2\%$. The matrix covers the full void fraction range, thus containing $n' = (\alpha_{max} - \alpha_{min})/\Delta\alpha = 50$ columns in the stratified flow regime.

The data have been reconstructed by the use of a long cycle K (27 fields) and a short cycle C (8 fields). Figure 5 shows, that the accuracy obtained with the short cycle C is not significantly poorer than the one obtained with the long cycle K, although the measurement rate is about 3 times higher. The average accuracy with the practical short cycle is in the region of 3%.

By increasing both gas and liquid flow rates and changing the smooth stratified flow to wavy flow, the reconstruction showed no noticeable deterioration. This effect is thought to be explained by the fact, that the wavelength of the surface waves on the liquid interface was short in relation to the length of the impedance probe. Therefore, the probe can be regarded as a low-pass filter with an averaging effect on the local void fraction fluctuations inside the probe. By reducing the electrode length to a value which is determined by the resolution of the impedance meter, and use of axial guarding electrodes, these fluctuations can be tracked.

### 4.2. Bubble flow

The reconstruction results for the bubble flow regime are shown in Fig. 6. In this regime, the reference matrix was generated by calibration in vertical, upward bubble flow of water and gas. The reference mean void fraction inside the test section was measured with two coupled, synchronously actuated ball valves, mounted 10 m apart. Preceding tests [10] showed an error margin of less than 2% within the covered void fraction span $0 \leqslant \alpha \leqslant 0.35$.

The results (Fig. 6) have been reconstructed by use of a short cycle Q (4 fields) and, again, the long cycle K (27 fields). Again, a very good performance is demonstrated. The average error margin with the short cycle is in the region of 2%

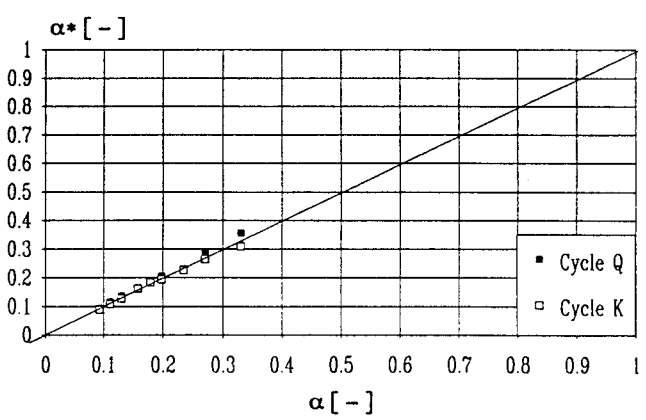


Fig. 6. Calculated ($\alpha^*$) vs. reference void fraction ($\alpha$) for bubble flow of water/gas. (Cycle Q: 4 fields: $D_3, E_6, B_4, M_1$; Cycle K: 27 fields.)

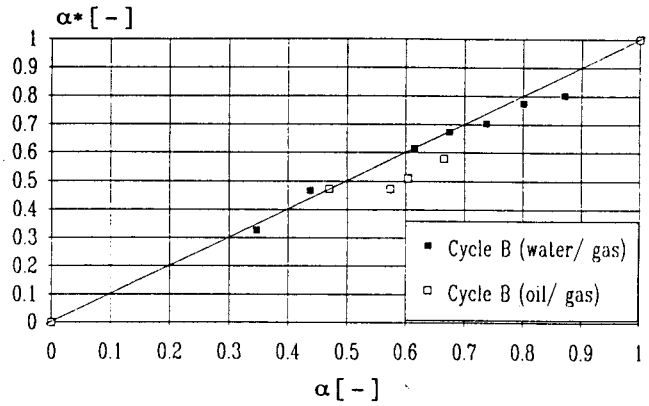


Fig. 7. Calculated ($\alpha^*$) vs. reference void fraction ($\alpha$) for annular flow of water/ gas. and oil/ gas. (Cycle B: 4 fields: $D_1$–$D_4$.)

and thus approaches the error of the reference measuring method; the measurement rate for cycle Q is over 3 $s^{-1}$.

### 4.3. Annular flow

Another regime of high importance to many applications is the annular flow regime. The reconstruction performance in this domain has been tested within a void fraction span of $0.35 \leqslant \alpha \leqslant 0.81$. The liquid superficial velocity was therefore set to $w_{s,l} = 1.8$ $ms^{-1}$, gas velocity was changed within the range $1.4 \leqslant w_{s,g} \leqslant 4.5$ $ms^{-1}$. Figure 7 shows the reconstructed data for oil/gas and water/gas flows, each calculated with a short cycle B, containing only the 4 diametral fields $D_1$–$D_4$ (see Fig. 2). The average error in oil/gas flow is about 9%, and thus significantly higher than in water/gas with 2.2%. The explanation to this lies in the different generation ways for the reference matrices for the two cases. The matrix for oil/gas flow was generated with the help of the stationary calibration apparatus, while the one for water/gas was calibrated in real annular flow.

For the stationary calibration procedure, 6 different void fraction points were generated inside the impedance probe. However, with this setup, the whole liquid was located around the pipe wall and no entrained liquid could be simulated. If impedance vectors measured in real annular flows are compared to a reference matrix generated in

the described way, this "wrong" calibration will result in a systematical error tending towards lower values, as shown in Fig. 7. This clearly shows, that calibration in real flows should be preferred to the stationary calibration, whenever possible.

## 5. Discussion and conclusions

The results presented in this paper demonstrate the excellent performance of the new developed, impedance-based reconstruction technique for multiphase flows. This improved technique avoids the disadvantages of the conventional impedance method – i.e. its sensitivity to the flow pattern – by multi-channel measurement with the help of numerous fields and a non-intrusive, multi-electrode probe. All the calculation steps and control functions for the impedance meter are easily performed by a regular-size PC. The new method detects the occurring flow regime and calculates the volumetric flow composition. Its application range can also be extended to 3-phase flows.

The required reference matrix can either be generated by numerical computation or by calibration. The best results (void fraction error margin 2%) are obtained by calibration in the real flow.

For every flow regime, special, dedicated measurement cycles can be found, which are composed of a low number of measuring fields, thus enabling a high measurement rate at good reconstruction accuracy. The setup used for the presented tests allowed for measurement rates of up to 4 $s^{-1}$, which can be considerably speeded up by use of a faster impedance meter.

## 6. List of used symbols

| | |
|---|---|
| $C$ [F] | capacitance, |
| $C^*$ [-] | rel. capacitance, |
| $l$ [m] | length of probe, |
| $M$ | matrix, |
| $Q$ [As] | charge, |
| $s$ [-] | error value, |
| $V$ | vector |
| w [$ms^{-1}$] | velocity, |
| $x,y$ | Cartesian coordinates, |
| $Z$ [$\Omega$] | impedance, |
| $\varnothing$ [m] | diameter of probe, |
| $\alpha$ [-] | void fraction, |
| $\varepsilon$ [-] | permittivity, |
| $\varrho$ [As $m^{-3}$] | space-charge density, |
| $\sigma$ [$\Omega^{-1}m^{-1}$] | specific conductivity, |
| $\varphi$ [V] | potential, |
| $\psi$ [-] | angle. |

### 6.1. Indices

| | |
|---|---|
| g | gas, |
| $i$ | row, |
| $j$ | column, |
| $l$ | liquid, |
| s | superficial. |

## 7. References

[1] H. Auracher and J. Daubert, 2nd Int. Conf. on Multi-Phase Flow, London, 1985.
[2] M.R. Özgü and J.C. Chen, Rev. Sci. Instrum. 44, No. 12 (1973) 1714–1716.
[3] J.M. Geraets and J.C. Int. J. Multiphase flow 14, No. 3 (1988) 305–320.
[4] M. Abouelwafa and J.M. Kendall, IEEE Trans. Instr. Meas., Vol. IM-29, No. 1 (1980) 24–27.
[5] M. Merilo, R.L. Dechene and W.M. Cichowlas, Trans. ASME J. Heat Transfer 99 (1977) 330–332.
[6] J.C. Maxwell, A Treatise on Electricity and Magnetism, Vol. 1 (Clarendon Press, Oxford, 1892), p. 452.
[7] D.A.G. Bruggeman, Ann. d. Physik, Vol. 24, No. 5 (1935) 636–679.
[8] L.K. van Beek, Dielectric behaviour of heterogeneous systems, in: Progress in Dielectrics, Vol 7 (1967).
[9] E. Dykesteen et al., J. Phys. E.: Sci. Instrum. 18 (1985) 540–544.
[10] F. Klug, Ein Messverfahren zur impedanzgestützten Rekonstruktion der Gemischzusammensetzung in Mehrphasenströmungen, Diss., Technische Universität München (1993).
[11] M.S. Bair and J.P. Oakley, 1st Meeting European Concerted Action on Process Tomography, Manchester, March 26–29, 1992 (1992).
[12] F. Klug and F. Mayinger, Proc. NURETH-5 Meeting, Salt Lake City, Sept. 21–24, 1992 (1992).
[13] E. Philippow, Grundlagen der Elektrotechnik, 8. Aufl. (Hüthig Verlag, Heidelberg, 1989).